AIAA JOURNAL
Vol. 46, No. 2, February 2008

Comparison of Open and Choked Premixed Combustor Exits During Thermoacoustic Limit Cycle

Peter A. Hield* and Michael J. Brear†
University of Melbourne,
Melbourne, Victoria 3010, Australia

DOI: 10.2514/1.32650

This paper compares the thermoacoustic limit cycles of a premixed laboratory combustor with acoustically open and choked exits. It is shown that the form of the downstream boundary condition can have a significant effect on the combustion chamber acoustics, with both the dominant limit cycle frequencies and the acoustic mode shapes being very different for the different combustor exits. The fundamental limit cycle frequency with the choked exit in place agrees closely with that determined by the convective time scales of entropy disturbances, as argued by other authors. A novel experimental method is then developed to examine the acoustic response of an arbitrary duct termination to incident pressure and entropy perturbations, and used to measure the response of the combustor downstream boundary condition during thermoacoustic limit cycle. The reflection coefficient for the acoustically open exit matches closely the classical result for zero mean flow. It is also shown that a choked nozzle downstream of the flame generates significant sound due to the interaction of the convected entropy perturbation with the nozzle. This final result is qualitatively in keeping with an existing analytic boundary condition for a choked nozzle, even though quantitative agreement is not observed. Reasons for this discrepancy are then suggested.

Nomenclature

A	=	Fourier transform of the nondimensional incident pressure fluctuation
AR	=	downstream nozzle area ratio
a	=	amplitude of the incident nondimensional pressure fluctuation
B	=	Fourier transform of the nondimensional reflected pressure fluctuation
b	=	amplitude of the reflected nondimensional pressure fluctuation
C_{ij}	=	real part of the cross-spectral density between i and j
c	=	speed of sound
c_p	=	specific heat at constant pressure
f	=	frequency
H	=	transfer function
k	=	wave number
L	=	length of rig downstream of the flame holder
M	=	Mach number
n	=	mode number
P	=	Fourier transform of the nondimensional pressure fluctuation
p	=	pressure
Q_{ij}	=	imaginary part of the cross-spectral density between i and j
R	=	reflection coefficient
S	=	Fourier transform of the nondimensional entropy fluctuation
S_{ij}	=	cross-spectral density between i and j
s	=	entropy, amplitude of the nondimensional entropy fluctuation
T	=	temperature, Fourier transform of the nondimensional temperature, measurement period
t	=	time
u	=	velocity
x	=	spatial coordinate
γ	=	ratio of specific heats
ρ	=	density
ϕ	=	equivalence ratio
ω	=	angular frequency

Subscripts

H	=	hot flow quantity
i	=	incident
n	=	mode number
p	=	pressure
r	=	reflected
s	=	entropy
1,2,...	=	measurement location, transfer function number

Modifiers

$\bar{g}$	=	mean component of the quantity g
g'	=	fluctuating component of the quantity g
g^*	=	complex conjugate of the complex number g

I. Introduction

THERMOACOUSTIC oscillations can occur whenever combustion takes place within a confined space. Unsteadiness in the heat release produces disturbances in the flow, which can then perturb the flame, generating more unsteady heat release. A mechanism explaining this phenomenon was first described by Rayleigh [1]. In applications such as gas turbine or rocket engines, the pressure fluctuations may become so intense that structural damage occurs.

Thermoacoustic oscillations in premixed combustors have been studied extensively over several decades [2,3]. However, most studies have concentrated on combustors with acoustically open exits, with the effect of choking the combustor exit receiving less attention [4]. This is an important omission, given that several theoretical studies suggest that a choked downstream boundary condition can have a strong effect on the system stability

Presented as Paper 494 at the 13th AIAA/CEAS Aeroacoustics Conference, Rome, 21–23 May 2007; received 6 June 2007; revision received 30 September 2007; accepted for publication 1 October 2007.

*Ph.D. Student, Department of Mechanical and Manufacturing Engineering, Parkville.

†Senior Lecturer, Department of Mechanical and Manufacturing Engineering, Parkville.

[4–6] and also that most in-service combustors feature choked or nearly choked nozzles immediately downstream of the combustion chamber.

Marble and Candel [7] developed a linear boundary condition for a choked nozzle, which is commonly used to model thermoacoustic instability. MacQuisten and Dowling [4] experimentally and theoretically studied the thermoacoustic instability inside a model afterburner, comparing an open exit and a choked exit nozzle. They find that the addition of the choked nozzle is highly destabilizing, and significantly changes the observed instability. They then use Marble and Candel's boundary condition coupled with a flame model developed by Bloxsidge et al. [8] and obtain reasonable agreement between the measured and experimental pressure mode shapes and the heat release. However, the comparison of choked and open combustor exits was not the main focus of the paper. Dowling [5] theoretically examined instability in a one-dimensional combustion chamber, using Marble and Candel's boundary condition and comparing two flame models, showed that a downstream nozzle can be a source of acoustic energy, leading to instability even though the Rayleigh energy source term is zero. She also shows that the presence of the nozzle can lead to a low-frequency mode depending on the convection time of the entropy disturbance. The existence of a low-frequency mode was also predicted by Keller [9], who developed a model predicting the frequency of an instability dominated by the convection time scales of entropy perturbations. In their experimental studies of low-frequency instability in diffusion combustors, Eckstein et al. [10] reached the opposite conclusion that the choked nozzle has no effect on the observed instability, which is instead dominated by the convection time scale of fuel droplets from the fuel atomizer to the flame front. It is likely that these conflicting results are due to the differing designs of the combustors: that of MacQuisten and Dowling [4] is a tube combustor with a bluff body stabilized flame, in which it is likely that combustion occurs over a long length extending almost to the downstream boundary, whereas in that of Eckstein et al. [10], combustion occurs over an axial length much shorter than the combustion chamber, allowing the entropy perturbation generated by the flame to diffuse before reaching the downstream boundary. Nevertheless, these differing views on the importance of the downstream boundary suggest that further investigation is required.

This paper compares the thermoacoustic limit cycles of a premixed laboratory combustor with acoustically open and choked exits. The comparisons include analysis of the duct acoustics with unsteady pressure transducers, and it is shown that the form of the downstream boundary condition can have a significant effect. Although Marble and Candel's [7] boundary condition is commonly used in theoretical studies, to the authors' knowledge, this boundary condition has not been experimentally verified. To investigate the downstream boundary condition further, the so-called "two-microphone method" [11] is extended to include incident convected entropy fluctuations, allowing the experimental determination of the response of an arbitrary duct termination to incident pressure and entropy perturbations. This method is then used to compare the response of the open and choked combustor exits, and it is shown that the choked nozzle generates significant upstream traveling pressure waves due to the interaction of the incident convected entropy perturbation with the combustor exit nozzle.

II. Experimental Methods

A. Combustion Rig Setup

The experimental rig is shown in Fig. 1. The working section is approximately axisymmetric, consisting of a 1-m long straight tube with a bluff body flame holder positioned on the midpoint of the duct axis. A 450-mm long section immediately downstream of the flame holder can be either fused quartz tube, to allow optical access to the flame, or stainless steel pipe, to allow pressure transducers to be mounted in the duct wall. The working section is fed with air from a dedicated 60-hp Sullair compressor and liquid petroleum gas (LPG, 98% propane) from cylinders. The fuel is injected into the air flow sufficiently far upstream of the working section to allow for complete mixing before the flame holder. The airflow rate, and hence the Mach number in the upstream half of the working section, is controlled by using a throttle valve to set the pressure upstream of the working section inlet nozzle. The fuel flow rate, and hence the equivalence ratio of the mixture, is set using a needle valve in the fuel line. An exhaust scoop removes the exhaust gases from the test cell, and was designed to be sufficiently far from the combustor exit so as to replicate an infinite volume as closely as possible within the confines of the test cell [12].

Broadly speaking, there are two forms of boundary conditions available for either end of the rig: an open inlet/exit, with the working section connected to a large volume, or a choked nozzle. Numerical studies using the model described in Dowling [13] were used as the basis for specifying the boundary conditions. This model determines the frequency and stability of thermoacoustic oscillations in a simple one-dimensional duct containing a flame. The calculations suggest that the system behaves in a similar manner for both open and choked upstream boundary conditions [6]. Thus it was decided that it was not necessary to allow for both possible upstream boundary conditions, and the rig was designed to have a choked boundary condition at the upstream end. The same calculations also suggested that the downstream boundary condition has a large effect on the system, and, in particular, on the system stability [6]. This finding is consistent with the findings of [4,14]. This is an important effect that is only mentioned briefly in the literature, and it is an aim of this study to investigate this effect further. Thus the rig was designed to allow the downstream end to be either open or choked.

The choked boundary condition was implemented using a plate with an angular array of small holes, to achieve uniform flow as quickly as possible downstream of the nozzle. The downstream boundary condition was set using a short removable section. This allowed the nozzle area ratio (AR, defined as the ratio of the throat area to the duct area) to be varied from open (AR = 1) to choked, the latter of which was achieved using a nozzle with AR = 0.1.

The acoustic pressure fluctuations inside the combustor were measured using Kulite WCT-312M fast response water-cooled pressure transducers, mounted with the pressure sensitive face flush with the internal wall of the combustion chamber. Seven mounting points were available (Fig. 2) allowing measurements along the length of the working section. The transducer signals were logged using a National Instruments PCI 6013e data acquisition card mounted in a PC. For all measurements in this paper, 60 s of data were taken, in six separate records of 10 s each, at a sample rate of 4096 Hz. Sensitivity studies showed that this sampling rate and duration accurately captured the characteristics of the duct acoustics.

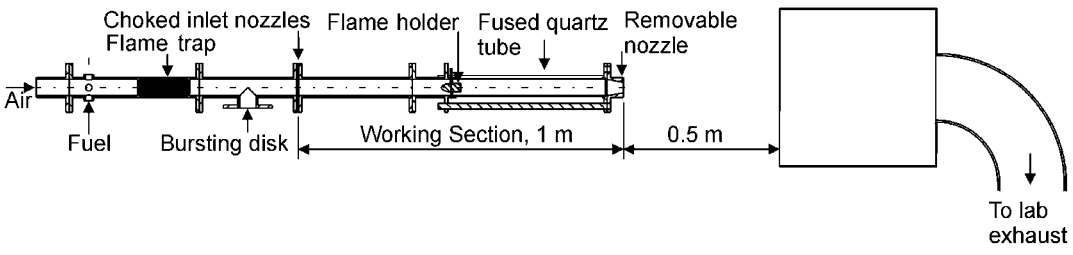

Fig. 1 A cross-section view of the experimental rig, showing the working section and the exhaust duct.

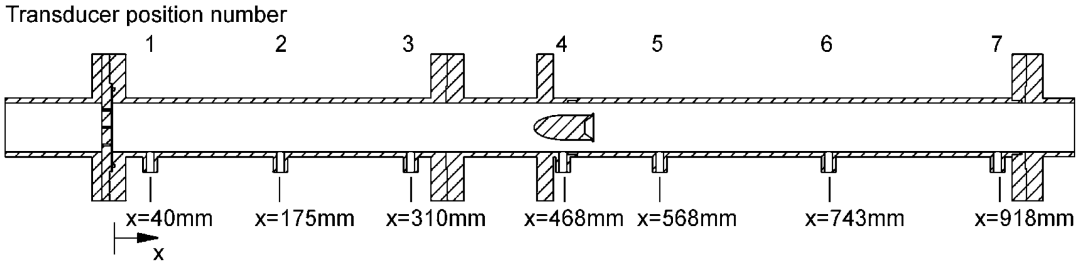

Fig. 2 Cross-section view of the working section, showing the locations of the pressure transducer mounting points, and an open exit.

Because the fuel was introduced upstream of the choked nozzles, there could be no equivalence ratio fluctuations entering the flame, and this effect could be discounted as a source of entropy fluctuations. However, entropy fluctuations were still present downstream of the flame, due to the interaction between the flame and the acoustic fluctuations (see, for example, [4–6,13]).

B. Two-Microphone and One Thermocouple (2M1T) Method

It is shown later that the combustor exit boundary condition can have a significant effect on the system stability. This is due to the different responses of the combustor exit boundary conditions to incident fluctuations. An open exit reflects pressure waves, while allowing entropy fluctuations to convect out of the duct, whereas entropy fluctuations convected through a nozzle can generate sound (e.g., [7,15]). In particular, a choked nozzle downstream of a flame can have a destabilizing effect (see, for example, [4,10,14]). Marble and Candel [7] examined the response of nozzles to convected gas nonuniformities and developed a linear exit boundary condition for a choked nozzle. For a compact nozzle, it takes the form

$$\frac{p'}{\bar{p}} = \frac{2u'}{\bar{u}} + \frac{\rho'}{\bar{\rho}} \tag{1}$$

This boundary condition captures the coupling between incident acoustic and entropic disturbances and a reflected acoustic disturbance. Although it has been widely used in studies of thermoacoustic instability [4–6,10,16], to the authors' knowledge it has not been experimentally verified.

Verification of this boundary condition may be attempted by an extension of one of the two separate formulations of the two-microphone method developed by Seybert and Ross [11] and Chung and Blaser [17]. These methods are essentially equivalent and use measurements from two wall-mounted microphones to determine the response of an acoustic impedance to incident pressure waves. Both methods are commonly used. The method of Seybert and Ross [11] has been used, for example, by Eldredge and Dowling [18] to determine the sound absorbed by a perforated duct liner, and by Jeong and Ih [19] to study the propagation of sound through a bundle of capillary tubes. No method is presently available, however, for determining the properties of a duct termination that can respond to both incident pressure waves and incident entropy fluctuations.

Assume that a duct termination has the geometry shown in Fig. 3. The duct contains a fluid moving at a mean velocity $\bar{u}$, and there is a downstream traveling pressure wave

$$\frac{p_i(x,t)}{\bar{p}} = a(t)e^{i(\omega t - k_i x)} \tag{2a}$$

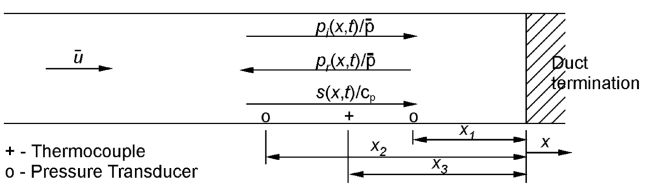

Fig. 3 A duct with an unknown termination, with a mean flow, incident pressure and entropy fluctuations, and a reflected pressure fluctuation.

and a convected entropy fluctuation moving with the mean flow

$$\frac{s(x,t)}{c_p} = s(t)e^{i(\omega t - k_s x)} \tag{2b}$$

These fluctuations interact with the duct termination to produce an upstream traveling pressure wave

$$\frac{p_r(x,t)}{\bar{p}} = b(t)e^{i(\omega t + k_r x)} \tag{2c}$$

In the above equations, k_i is the downstream traveling wave number

$$k_i = \frac{\omega}{\bar{c} + \bar{u}}$$

k_r is the upstream traveling wave number

$$k_r = \frac{\omega}{\bar{c} - \bar{u}}$$

and k_s is the "wave number" of the entropy fluctuation

$$k_s = \frac{\omega}{\bar{u}}$$

The duct termination is assumed to be a linear, multi-input single-output (MISO) system, with the amplitudes of the incident nondimensional pressure and entropy fluctuations (a and s) as inputs, and the amplitude of the reflected nondimensional pressure fluctuation (b) as the output (see Fig. 4). For this system, it can be shown that (e.g., Newland [20])

$$S_{ab}(\omega) = S_{aa}(\omega)H_1(\omega) + S_{as}(\omega)H_2(\omega) \tag{3a}$$

and

$$S_{sb}(\omega) = S_{sa}(\omega)H_1(\omega) + S_{ss}(\omega)H_2(\omega) \tag{3b}$$

where $H_1(\omega) = R_p = P_{rp}(\omega)/P_i(\omega)$ is the transfer function between the incident pressure fluctuation and the reflected pressure fluctuation due to the incident pressure fluctuation (the pressure reflection coefficient) and $H_2(\omega) = R_s = P_{rs}(\omega)/S(\omega)$ is the transfer function between the incident entropy fluctuation and the reflected pressure fluctuation due to the incident entropy perturbation (the entropy reflection coefficient), and $S_{ij}(\omega)$ is the cross-spectral density between i and j at $x = 0$. The total reflected pressure wave is then the sum of these two components

$$P_r(\omega) = H_1(\omega)P_i(\omega) + H_2(\omega)S(\omega) \tag{4}$$

It is noted that R_s is not strictly a reflection coefficient, as the incident entropy disturbance is not reflected by the nozzle, but instead produces a pressure disturbance that propagates upstream. However, the term "entropy reflection coefficient" follows from the term "pressure reflection coefficient" and is used throughout this paper.

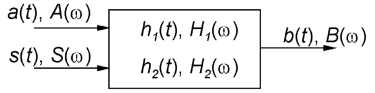

Fig. 4 Block diagram showing the transfer functions between the acoustic velocity and temperature and the acoustic pressure.

Equations (3a) and (3b) can be solved simultaneously to yield the transfer functions

$$H_1(\omega) = \frac{S_{sb}(\omega)S_{as}(\omega) - S_{ss}(\omega)S_{ab}(\omega)}{S_{as}(\omega)S_{sa}(\omega) - S_{ss}(\omega)S_{aa}(\omega)} \tag{5a}$$

and

$$H_2(\omega) = \frac{S_{sa}(\omega)S_{ab}(\omega) - S_{aa}(\omega)S_{sb}(\omega)}{S_{sa}(\omega)S_{as}(\omega) - S_{aa}(\omega)S_{ss}(\omega)} \tag{5b}$$

As Fig. 3 shows, the pressure in the duct is measured at two points x_1 and x_2 and the temperature is measured at one point x_3. For linear disturbances in a homogeneous flow, the measured pressures and temperature fluctuations are given by [13]

$$\frac{p_1(x_1,t)}{\bar{p}} = [a(t)e^{-ik_i x_1} + b(t)e^{ik_r x_1}]e^{i\omega t} \tag{6a}$$

$$\frac{p_2(x_2,t)}{\bar{p}} = [a(t)e^{-ik_i x_2} + b(t)e^{ik_r x_2}]e^{i\omega t} \tag{6b}$$

$$\frac{T_3(x_3,t)}{\bar{T}} = \left[\frac{(\gamma-1)}{\gamma}[a(t)e^{-ik_i x_3} + b(t)e^{ik_r x_3}] + s(t)e^{-ik_s x_3}\right]e^{i\omega t} \tag{6c}$$

and the Fourier transforms of these measurements are

$$P_1(\omega,T) = e^{-ik_i x_1}A(\omega,T) + e^{ik_r x_1}B(\omega,T) \tag{7a}$$

$$P_2(\omega,T) = e^{-ik_i x_2}A(\omega,T) + e^{ik_r x_2}B(\omega,T) \tag{7b}$$

$$T_3(\omega,T) = \frac{(\gamma-1)}{\gamma}[e^{-ik_i x_3}A(\omega,T) + e^{ik_r x_3}B(\omega,T)] + e^{-ik_s x_3}S(\omega,T) \tag{7c}$$

The auto- and cross-spectral densities of the measured pressures and temperature can be estimated from the measured data by (e.g., Bendat and Piersol [21])

$$S_{11} = \frac{1}{T}P_1^*(\omega,T)P_1(\omega,T) \tag{8a}$$

$$S_{22}(\omega,T) = \frac{1}{T}P_2^*(\omega,T)P_2(\omega,T) \tag{8b}$$

$$S_{12}(\omega,T) = \frac{1}{T}P_1^*(\omega,T)P_2(\omega,T) \tag{8c}$$

$$S_{13}(\omega,T) = \frac{1}{T}P_1^*(\omega,T)T_3(\omega,T) \tag{8d}$$

$$S_{23}(\omega,T) = \frac{1}{T}P_2^*(\omega,T)T_3(\omega,T) \tag{8e}$$

and

$$S_{33}(\omega,T) = \frac{1}{T}T_3^*(\omega,T)T_3(\omega,T) \tag{8f}$$

Substituting Eqs. (7a–7c) into Eqs. (8a–8f), and writing the real and imaginary parts separately gives a system of nine equations relating the auto- and cross-spectral densities of the measured pressure and temperature fluctuations to the auto- and cross-spectral densities of the incident and reflected wave amplitudes. This system of equations can then be solved for S_{aa}, S_{bb}, S_{ab}, S_{as}, S_{bs}, and S_{ss}, and Eqs. (5a) and (5b) can then be used to obtain the transfer functions $H_1(\omega)$ and $H_2(\omega)$. The full form of these equations is given in the Appendix.

C. Implementation of the 2M1T Method

As with the pressure transducer measurements described above, 60 s of data were taken in six separate records of 10 s each at a sample rate of 4096 Hz. For the determination of the pressure and entropy reflection coefficients, it was necessary to estimate the auto- and cross-spectral densities S_{11}, S_{22}, S_{12}, S_{13}, S_{23}, and S_{33} from the measured data. To do this, MATLAB's cross-power spectral density (cpsd) function was used. Each 10 s record was split into 65 overlapping 2.5 s subrecords, and the cpsd function is applied to each subrecord. The cpsd function further splits each subrecord into eight segments overlapping by 50%, applies a Hamming window to each segment, and uses Welch's averaged, modified periodogram method to estimate the auto- or cross-spectral density [22]. Because of the averaging method used, splitting the data records in this way results in a spectral resolution of 1 Hz in the estimated spectral densities. The separate spectral densities are then averaged before being used in the calculation of S_{aa}, S_{bb}, S_{ab}, S_{as}, S_{bs}, and S_{ss}.

A type "R" (platinum/platinum-13% rhodium) thermocouple was used to measure the temperature fluctuations. The thermocouple was constructed from unsheathed 50 μm diameter wire, threaded through twin bore ceramic tubing attached to a swagelok fitting and mounted in the duct wall in the same plane as pressure transducer location 7. The thermocouple junction was created by welding the wires with an oxy-acetylene torch, and was flattened in a press to further decrease the junction's volume to surface area ratio and hence its time constant. Figure 5 shows a cross-sectional view of the thermocouple mount and a photograph of the thermocouple tip. A similar thermocouple was used by Dawson and Fitzpatrick [23] to measure the temperature spectrum downstream of the flame in a dump combustor during thermoacoustic instability.

The frequency response of the thermocouple depends on the fluid in which the junction is immersed. Thus, the frequency response could only be reliably tested in the experimental rig during thermoacoustic instability. Several operating conditions were tested, and Fig. 6 shows typical results from the operating point AR = 0.4, $\bar{M} = 0.040$, and $\phi = 1.00$. Figure 6a shows the measured nondimensional pressure spectrum from transducer location 7, Fig. 6b shows the expected nondimensional acoustic temperature spectrum calculated by scaling the pressure measurement, and Fig. 6c shows the measured nondimensional temperature spectrum. The pressure spectrum has peaks at 180 and 355 Hz. The measured temperature spectrum has a peak at 180 Hz, which is not much smaller than the peak in the expected acoustic temperature spectrum, and a small peak a 355 Hz. This suggests that the thermocouple cutoff frequency is close to 180 Hz, and that temperature fluctuations below this frequency can be measured with reasonable accuracy. There is also significant energy in the measured temperature

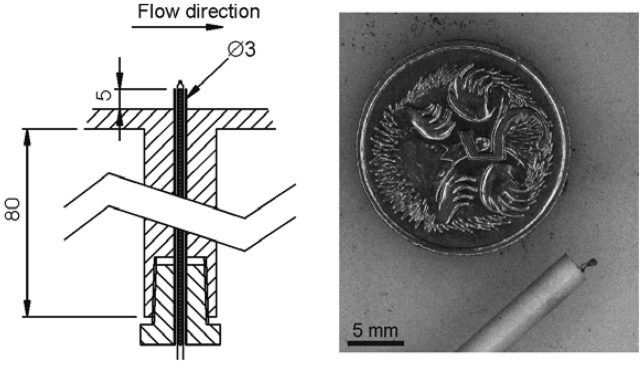

a) b)

Fig. 5 a) Cross-section view of the thermocouple mount, and b) a photograph of the thermocouple tip.

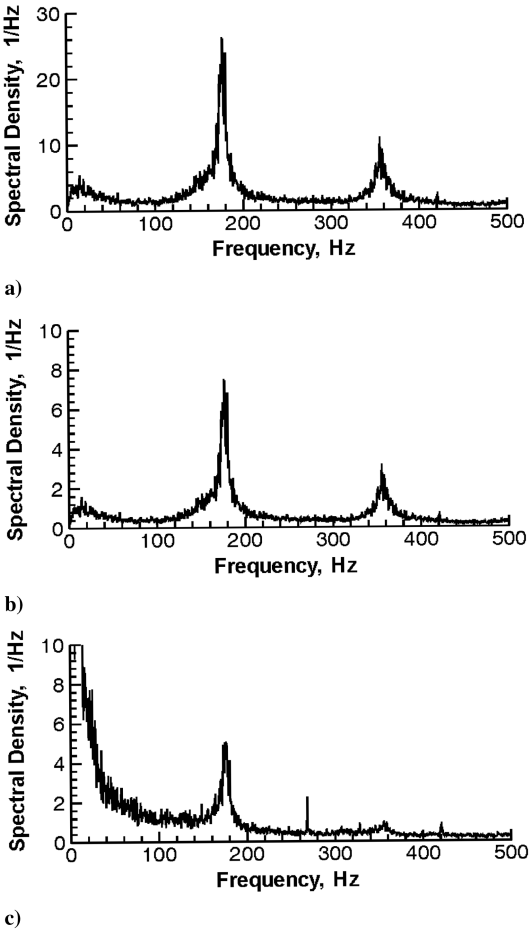

Fig. 6 Spectra from transducer location 7 at the operating point AR = 0.4, $\bar{M} = 0.040$, $\phi = 1.00$. a) Pressure spectra, b) acoustic temperature spectra calculated from the pressure measurement, and c) measured temperature spectra.

spectrum at low frequencies, which is most likely due to low-frequency fluctuations in the heat release from the flame. Low-frequency fluctuations were also seen in separate measurements of the heat release [12] and in the temperature measurements of Dawson and Fitzpatrick [23].

A correction to the thermocouple frequency response was also investigated as part of this study and is fully explained in Hield [12]. This theoretical investigation, based on an energy balance of the thermocouple bead, showed that the thermocouple should accurately capture the temperature fluctuations below the cutoff frequency (approximately 200 Hz) without any amplitude or phase correction, and above this frequency, a correction amplified both the measured temperature fluctuations and the noise on the signal. Despite this conclusion, in [12] the 2M1T method was applied to the corrected temperature data as well as the uncorrected, and the results compared. There were no significant differences in the calculated reflection coefficients in each case. Thus applying a correction did not improve the temperature data and has not been included here.

D. Validation of 2M1T Method

The 2M1T measurement technique was validated on test data representing a duct termination which fulfills Marble and Candel's [7] boundary condition [Eq. (1)]. To create the test data, the incident waves P_i and S at the duct termination were represented using a white noise data series. The reflected wave P_r was calculated using the appropriate reflection coefficients, and then all three waveforms were time shifted and added to obtain the pressure and temperature waveforms at the measurement locations. The reflection coefficients were then calculated from the test data using the method described here, and the results are shown in Fig. 7. The results are displayed for frequencies below 200 Hz, as this is the expected frequency range for which the thermocouple can accurately measure the temperature fluctuations. Below 20 Hz, there is significant error apparent in the reflection coefficient for the choked exit. For very low frequencies, the microphones will become compact and therefore measure the same pressure, making it harder to extract the separate waveforms, but above 20 Hz, the method reproduces the theoretical boundary condition. The duration of the test data series was 60 s, matching the experimental record length, and the nondimensional wave amplitudes $p_i/\bar{p}$ and s/c_p were equal. Numerical experiments were performed, varying both the record length and the relative amplitudes of the waves, and showed that the scatter in the result for $|R_s|$, in particular, is due to the duration of the test data and to the relative wave amplitudes. A 300 s of test data showed substantially less scatter, and increasing the relative amplitude of the entropy wave also reduced the scatter. Ultimately, the reasons for the differing scatter in $|R_p|$ and $|R_s|$ can only be speculated on in the absence of a full error analysis, which is a substantial task in itself, as discussed later. Nonetheless, the method appears capable of determining the pressure and entropy reflection coefficients in the range 20–200 Hz.

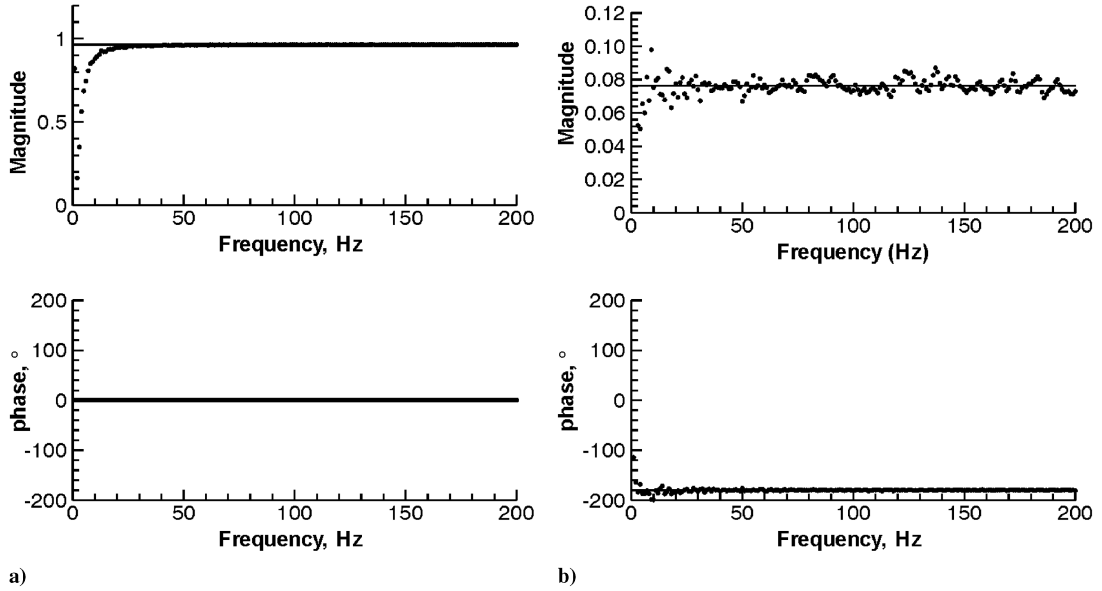

Fig. 7 Frequency dependence of R_p and R_s for a choked exit obeying Marble and Candel's [7] compact boundary condition. Analytic result (solid line), and the result determined from the test data (dots). a) Pressure reflection coefficient and b) entropy reflection coefficient.

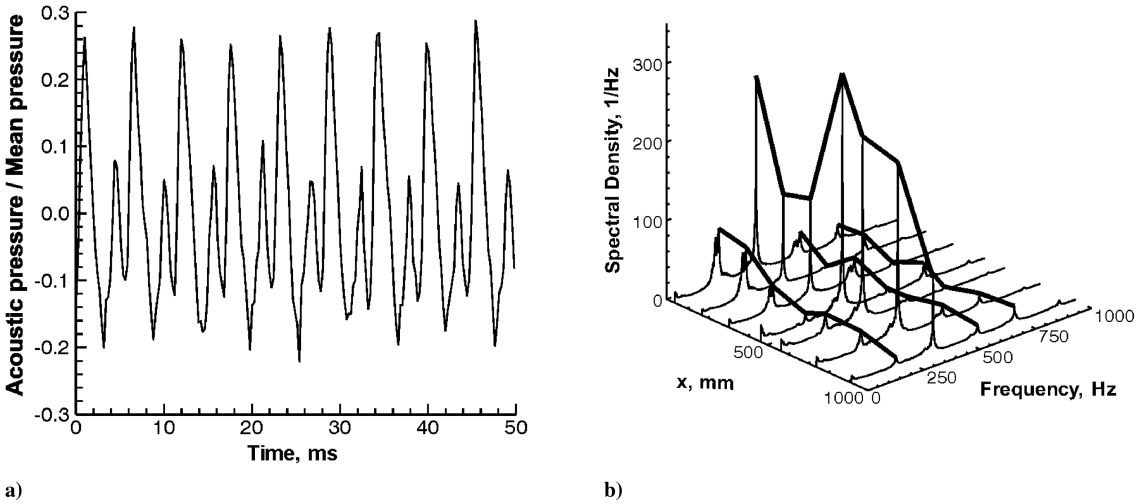

a) b)

Fig. 8 Pressure transducer results for AR = 1.0, $\bar{M} = 0.040$ and $\phi = 1.00$. a) A typical pressure trace from transducer position 1, and b) the pressure spectra for each transducer location, showing the frequencies of oscillation and the mode shapes.

III. Results and Discussion

A. Open Combustor Exit

Figure 8 shows the pressure transducer results from a typical operating point with an open exit. The pressure trace is from transducer position 1, immediately downstream of the inlet nozzle. The pressure trace at this location contains two main frequencies, with the first harmonic having the largest amplitude. The amplitude of the pressure waves is very large, reaching almost 30 kPa above the mean combustor pressure, which is atmospheric at this operating condition, and the peaks in the spectra are very clear above the background noise level. Assuming negligible mean flow, the upstream end of the working section is expected to be a pressure antinode, and the downstream end a pressure node, and this appears to be confirmed by the results. However, the frequencies beyond the fundamental do not correspond with the classical duct modes.

The results shown in Fig. 8 are replicated with minor variations over almost the whole available operating range, when the open exit is in place. The amplitude of the fluctuations increases slightly with Mach number and displays a peak at approximately stoichiometric values of the equivalence ratio. The relative size of the modes also varies slightly. The amplitude of the pressure fluctuations decreases rapidly below an equivalence ratio of about 0.85. These findings are consistent with the behavior observed in similar rigs [24,25].

B. Choked Combustor Exit

It was necessary to use a downstream nozzle with an area ratio of 0.1 to choke the exit of the working section at a Mach number of 0.034 upstream of the flame and an equivalence ratio of 0.78. As the total flow rate of fuel and air cannot be changed once the rig is operating, only a few choked exit operating points are possible. This section compares the rig characteristics at a choked exit operating point of $\bar{M} = 0.034$, $\phi = 0.78$ with the open exit operating point at the same Mach number and equivalence ratio as well as the results presented earlier.

Two seconds of raw pressure data are shown in Fig. 9, with data from the same operating point with an open combustor exit for comparison. In the open exit case, the mean pressure is atmospheric, and the rig is considered to be stable with only very low amplitude pressure fluctuations barely distinguishable from the background noise (see also Fig. 10a). The addition of the choked nozzle increases the mean pressure to 210 kPa and switches the rig from stable to unstable operation, with very large amplitude pressure fluctuations. This high mean absolute duct pressure can only be sustained by a choked downstream nozzle. Further, Fig. 9 shows clearly the effect of the downstream boundary condition. At this operating point, choking the combustor exit clearly causes a thermoacoustic limit cycle when at the same operating point with the open exit the

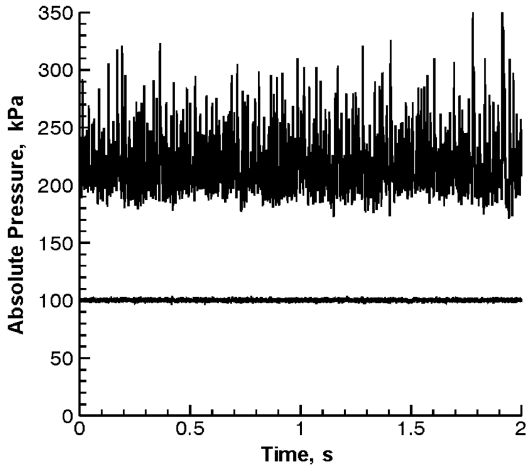

Fig. 9 Raw traces of absolute pressure for $\bar{M} = 0.034$, $\phi = 0.78$, with an open combustor exit (lower trace) and a choked combustor exit (upper trace).

combustor is stable. Clearly then, additional mechanisms are involved when the combustor exit is choked.

Figure 10 compares the nondimensional pressure fluctuations and the pressure spectra for the open and choked downstream boundary conditions in more detail. For the open exit case the amplitude of the oscillations is very small. With the choked exit nozzle, however, there is clear thermoacoustic instability, with the amplitude of the pressure fluctuations reaching roughly 30% of the mean pressure.

Although it is not a direct comparison, it is interesting to compare the behavior of the unstable cases for choked and open combustor exits. The pressure fluctuations at this choked exit operating point have a similar nondimensional amplitude as those at the unstable open exit operating point described earlier. It is noted that the mean pressure for the choked exit case is approximately double that in the open exit case, so the absolute amplitude of the pressure wave is approximately 60 kPa. In the choked case, the peak in the spectra is at a frequency lower than the fundamental acoustic frequency, and the mode shape is flat along the length of the duct, whereas the open exit spectra contain four clear modes (see Fig. 8).

Keller [9] proposed a mechanism of instability for combustion chambers with choked exits, in which the main driver of the instability is the upstream traveling acoustic wave generated as the entropy fluctuation from the flame convects through the downstream nozzle. The dominant time scale in this mechanism is the convection time of the entropy perturbation, which leads to oscillations at frequencies lower than those typical for acoustically driven

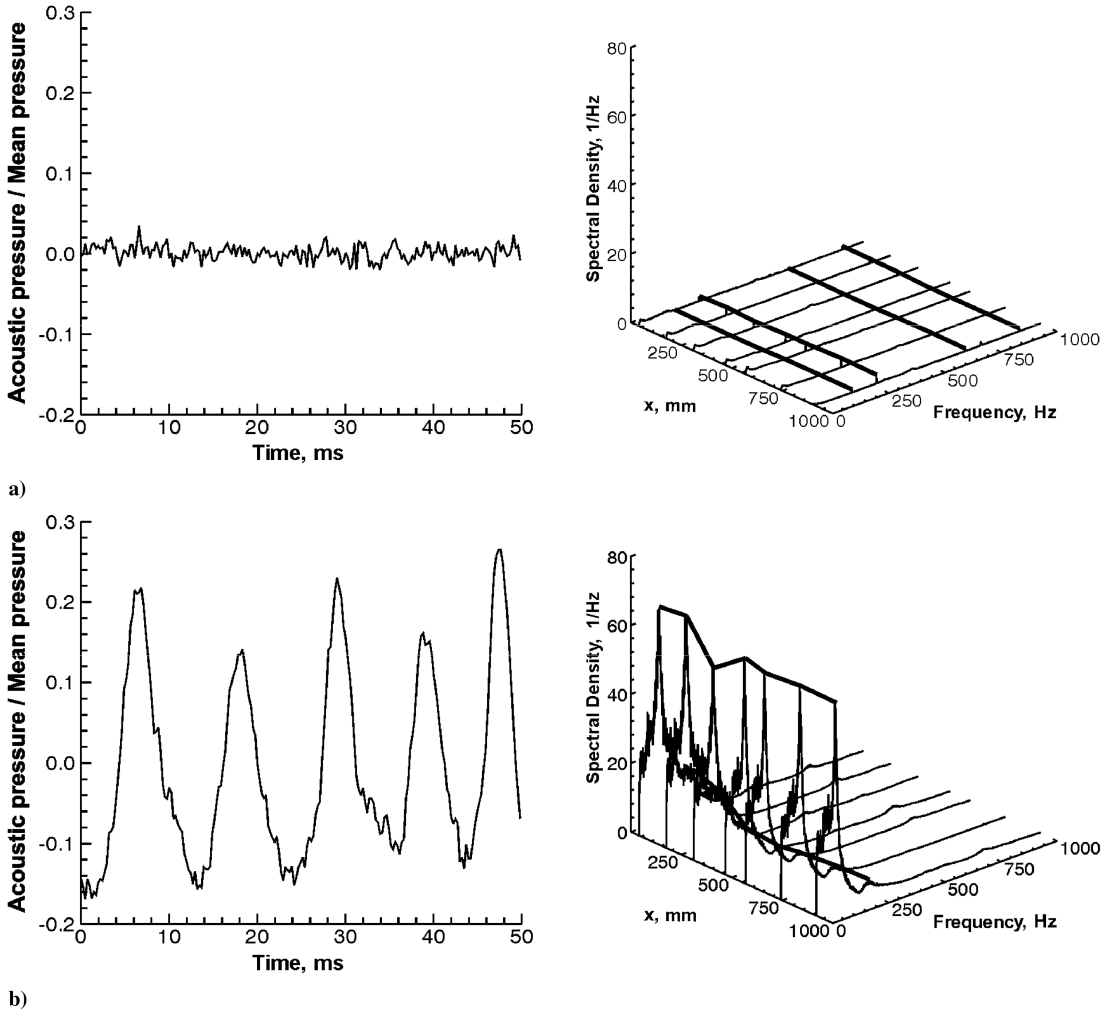

Fig. 10 Nondimensional pressure traces and spectra for $\bar{M} = 0.034$, and $\phi = 0.78$. a) Open exit, AR = 1.0, and b) choked exit, AR = 0.1.

instability. Keller derives an expression for the frequency of entropically driven oscillations,

$$f_n = (2n-1)\frac{u_H}{2L} + O(M_H u_H / L) \tag{9}$$

[Eq. (21) from [9]], where n is the mode number, L is the duct length downstream of the flame, and u_H and M_H are the hot gas velocity and Mach number, respectively. Further studies by the first author show that it is reasonable to calculate the velocity downstream of the flame based on the assumption of complete adiabatic combustion [12], giving $u_H = 84$ ms^{-1} for this operating condition. Using this value, together with $L = 0.5$ m, the equation predicts a fundamental frequency of 84 Hz, closely matching the experimentally measured frequency of 90 Hz shown in Fig. 10b.

C. Experimentally Measured Response of Combustor Exit

It was shown earlier that the combustor exit boundary condition can have a significant effect on the stability of the system. The 2M1T method is now used to investigate the response of a choked nozzle to incident pressure and entropy fluctuations. The pressure was measured at two locations upstream of the nozzle using two of the Kulite fast response pressure transducers mounted at locations 6 and 7 (see Fig. 2), and the temperature was measured at location 7 using the fast response thermocouple.

Theoretical pressure and entropy reflection coefficients for a compact choked nozzle can be derived from Marble and Candel's [7] boundary condition. The fluctuating quantities can be written in terms of the characteristics

$$\frac{p'}{\bar{p}} = \frac{p_i}{\bar{p}} + \frac{p_r}{\bar{p}}, \qquad \frac{u'}{\bar{u}} = \frac{1}{\gamma \bar{M}}\left(\frac{p_i}{\bar{p}} - \frac{p_r}{\bar{p}}\right)$$
$$\frac{\rho'}{\bar{\rho}} = \frac{1}{\gamma}(p_i + p_r) - \frac{s}{c_p} \tag{10}$$

and substituted into Eq. (1). Taking the Fourier transform and rearranging gives

$$P_r = \frac{2-(\gamma-1)\bar{M}}{2+(\gamma-1)\bar{M}} P_i - \frac{\gamma \bar{M}}{(2+(\gamma-1)\bar{M})} S \tag{11}$$

and therefore the reflection coefficients can be written as

$$R_p = \frac{P_{rp}}{P_i} = \frac{2-(\gamma-1)\bar{M}}{2+(\gamma-1)\bar{M}} \tag{12}$$

where P_{rp} is the reflected pressure perturbation due to the incident pressure perturbation, and

$$R_s = \frac{P_{rs}}{S} = -\frac{\gamma \bar{M}}{(2+(\gamma-1)\bar{M})} \tag{13}$$

where P_{rs} is the reflected pressure perturbation due to the incident entropy perturbation. Equations (12) and (13) are the transfer functions between the pressure wave propagated upstream from a compact choked nozzle and the incident pressure and entropy perturbations, respectively.

Figure 11 shows the measured (dots) and theoretical (solid line) pressure and entropy reflection coefficients for the open exit, at $\bar{M} = 0.034$, $\phi = 0.78$. The entropy reflection coefficient is roughly

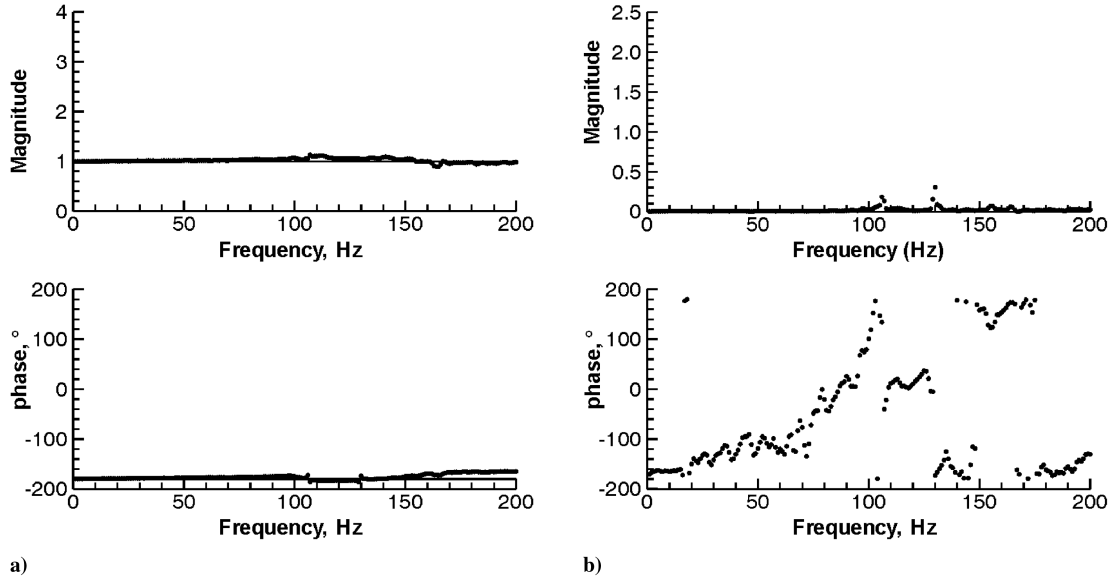

Fig. 11 Measured (dots) and theoretical (solid line) reflection coefficients for the open exit (AR = 1.0) at $\bar{M} = 0.034$, $\phi = 0.78$. a) Pressure reflection coefficient and b) entropy reflection coefficient.

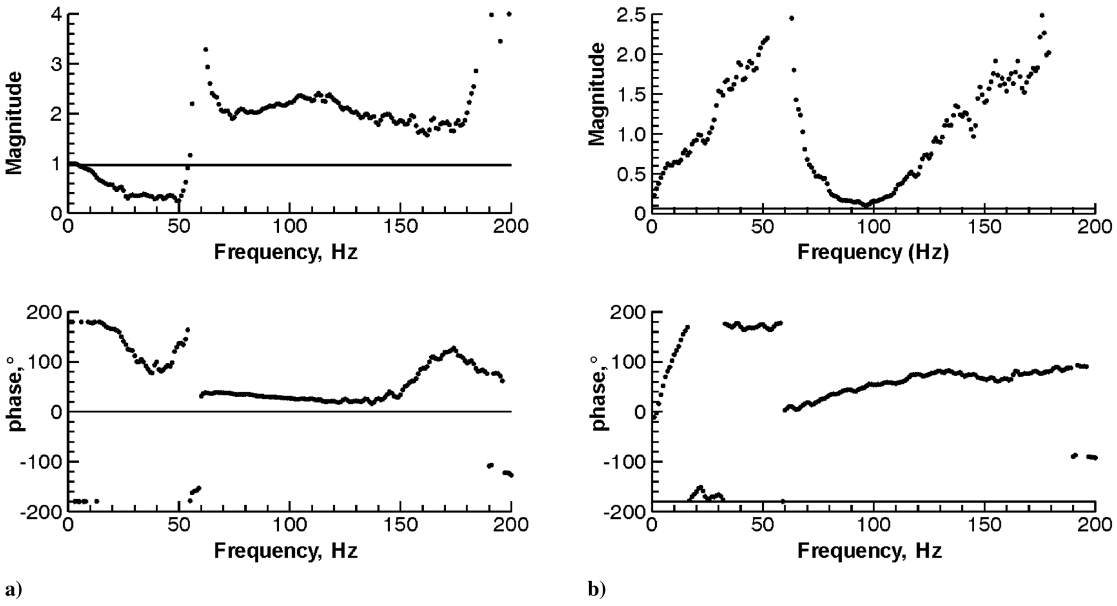

Fig. 12 Measured (dots) and theoretical [solid line, Eqs. (12) and (13)] reflection coefficients for the choked exit (AR = 0.1) at $\bar{M} = 0.034$, $\phi = 0.78$. a) Pressure reflection coefficient and b) entropy reflection coefficient.

zero for the open exit, as expected, and the pressure reflection coefficient is close to the classical result of $R_p = -1$.

The reflection coefficients are significantly different for the choked case (Fig. 12), and, in particular, the entropy reflection coefficient is at least 2 orders of magnitude greater than for the open case. This shows clearly that the form of the downstream boundary condition has a large effect on the system, and that a choked nozzle downstream of the flame is a source of acoustic energy.

The differences between the measured and theoretical results in Fig. 12 for both the pressure and entropy reflection coefficients have several probable sources. First, the narrowband forcing should create more experimental error away from the forcing frequencies, although it is difficult to conceive of an alternative experiment that could provide this forcing amplitude at arbitrary and controllable forcing frequencies. There are also general measurement errors as well as errors inherent to the 2M1T method. A thorough discussion of the influence of errors on the original two microphone methods is given in [26,27]. Such an analysis has not been attempted here, because the MISO approach of the 2M1T method makes this a substantial study in itself.

Further, it is possible that a choked downstream nozzle in a real system undergoing a thermoacoustic limit cycle, while just choked if only the mean conditions are considered, will in reality vary from strongly choked to unchoked as the pressure upstream of the nozzle varies throughout a cycle (see Figs. 9 and 10b). This effect was studied by Moase et al. [28], and caused significant nonlinearity in the boundary condition and a more complicated frequency response than the linear boundary condition proposed by Marble and Candel [7]. The proposed method for determining the reflection coefficients is inherently linear, thus potentially creating more errors when analyzing a nonlinear system. Also, although the duct acoustics are approximately one dimensional, the temperature field is not, so that a temperature measurement at a single point in space should not be expected to represent the temperature disturbance averaged over the duct area. Once again, such a measurement is challenging, requiring several probes suspended within an unstable flame.

Nonetheless, a comparison of the relative magnitudes of the entropic reflection coefficients in Figs. 11b and 12b shows that the choked nozzle does generate much more sound than the open exit. This entropic reflection coefficient is at least of the same order of

magnitude as that given by Marble and Candel's linear boundary condition, and further work should consider experimental validation of Marble and Candel's theory at lower forcing amplitude.

IV. Conclusions

This paper presented results from an experimental investigation of the acoustics in a premixed laboratory combustor during a thermoacoustic limit cycle. The form of the downstream boundary condition has been shown to have a significant effect on the combustion chamber acoustics, affecting both the modes present and the amplitude of these modes. In particular, a choked exit nozzle significantly alters the pressure spectrum inside the combustion chamber. With a choked nozzle in place, the spectral content is more broadband and of lower frequency, compared to the three or four distinct peaks present for the open exit at an unstable operating point. Further, the two results at the same operating point (defined by the Mach number upstream of the flame and the equivalence ratio) with the open exit and the choked exit nozzle resulted in a stable operation and a large amplitude thermoacoustic limit cycle, respectively. This showed clearly that changing the downstream boundary condition from open to choked can switch the rig between stable and unstable operating conditions.

The frequency response of the downstream boundary condition was therefore investigated in more detail. An experimental method was first developed to determine the response of an arbitrary duct termination to forcing by both incident pressure waves and incident entropy fluctuations, using measurements of the pressure fluctuations at two locations and the temperature fluctuations at one location. This method was applied to both the open exit and the choked exit nozzle. The open exit results agreed closely with classical theory. Although the results contained several likely sources of error due to the very challenging experimental environment, they also clearly showed that a choked nozzle forced by an incident entropy wave acts as a significant source of sound which propagates upstream.

Sound generated by the interaction of incident entropy disturbances with the choked nozzle was qualitatively in keeping with Marble and Candel's [7] linear boundary condition, although close quantitative agreement with this boundary condition was not observed. It was argued that this may be expected, given the large amplitude of the forcing and the possible nonlinearity of the choked exit due to periodic nozzle unchoking, as suggested recently by another study [28]. The application of Keller's [9] equation for the frequency of convective modes showed that the sound generated by the interaction of the entropy disturbance with the choked nozzle is the cause of the large difference in the acoustic spectra of the open and choked exit cases.

Appendix: Equations Relating the Cross-Power Spectral Densities

The full form of the equations relating the auto- and cross-spectral densities of the measured pressure and temperature fluctuations to the auto- and cross-spectral densities of the incident and reflected wave amplitudes are

$$S_{11} = S_{aa} + S_{bb} + 2C_{ab}\cos(k_i + k_r)x_1 - 2Q_{ab}\sin(k_i + k_r)x_1 \tag{A.1}$$

$$S_{22} = S_{aa} + S_{bb} + 2C_{ab}\cos(k_i + k_r)x_2 - 2Q_{ab}\sin(k_i + k_r)x_2 \tag{A.2}$$

$$\begin{aligned} C_{12} = {} & S_{aa}\cos k_i(x_1 - x_2) + S_{bb}\cos k_r(x_1 - x_2) \\ & + C_{ab}(\cos(k_i x_1 + k_r x_2) + \cos(k_r x_1 + k_i x_2)) \\ & - Q_{ab}(\sin(k_i x_1 + k_r x_2) + \sin(k_r x_1 + k_i x_2)) \end{aligned} \tag{A.3}$$

$$\begin{aligned} Q_{12} = {} & S_{aa}\sin k_i(x_1 - x_2) - S_{bb}\sin k_r(x_1 - x_2) \\ & + C_{ab}(\sin(k_i x_1 + k_r x_2) - \sin(k_r x_1 + k_i x_2)) \\ & + Q_{ab}(\cos(k_i x_1 + k_r x_2) - \cos(k_r x_1 + k_i x_2)) \end{aligned} \tag{A.4}$$

$$\begin{aligned} C_{13} = {} & \frac{(\gamma - 1)}{\gamma}(S_{aa}\cos k_i(x_1 - x_3) + S_{bb}\cos k_r(x_1 - x_3) \\ & + C_{ab}(\cos(k_i x_1 + k_r x_3) + \cos(k_r x_1 + k_i x_3)) \\ & - Q_{ab}(\sin(k_i x_1 + k_r x_3) + \sin(k_r x_1 + k_i x_3))) \\ & + C_{as}\cos(k_i x_1 - k_s x_3) - Q_{as}\sin(k_i x_1 - k_s x_3) \\ & + C_{bs}\cos(k_r x_1 + k_s x_3) + Q_{bs}\sin(k_r x_1 + k_s x_3) \end{aligned} \tag{A.5}$$

$$\begin{aligned} Q_{13} = {} & \frac{(\gamma - 1)}{\gamma}(S_{aa}\sin k_i(x_1 - x_3) - S_{bb}\sin k_r(x_1 - x_3) \\ & + C_{ab}(\sin(k_i x_1 + k_r x_3) - \sin(k_r x_1 + k_i x_3)) \\ & + Q_{ab}(\cos(k_i x_1 + k_r x_3) - \cos(k_r x_1 + k_i x_3))) \\ & + C_{as}\sin(k_i x_1 - k_s x_3) + Q_{as}\cos(k_i x_1 - k_s x_3) \\ & - C_{bs}\sin(k_r x_1 + k_s x_3) + Q_{bs}\cos(k_r x_1 + k_s x_3) \end{aligned} \tag{A.6}$$

$$\begin{aligned} C_{23} = {} & \frac{(\gamma - 1)}{\gamma}(S_{aa}\cos k_i(x_2 - x_3) + S_{bb}\cos k_r(x_2 - x_3) \\ & + C_{ab}(\cos(k_i x_2 + k_r x_3) + \cos(k_r x_2 + k_i x_3)) \\ & - Q_{ab}(\sin(k_i x_2 + k_r x_3) + \sin(k_r x_2 + k_i x_3))) \\ & + C_{as}\cos(k_i x_2 - k_s x_3) - Q_{as}\sin(k_i x_2 - k_s x_3) \\ & + C_{bs}\cos(k_r x_2 + k_s x_3) + Q_{bs}\sin(k_r x_2 + k_s x_3) \end{aligned} \tag{A.7}$$

$$\begin{aligned} Q_{23} = {} & \frac{(\gamma - 1)}{\gamma}(S_{aa}\sin k_i(x_2 - x_3) - S_{bb}\sin k_r(x_2 - x_3) \\ & + C_{ab}(\sin(k_i x_2 + k_r x_3) - \sin(k_r x_2 + k_i x_3)) \\ & + Q_{ab}(\cos(k_i x_2 + k_r x_3) - \cos(k_r x_2 + k_i x_3))) \\ & + C_{as}\sin(k_i x_2 - k_s x_3) + Q_{as}\cos(k_i x_2 - k_s x_3) \\ & - C_{bs}\sin(k_r x_2 + k_s x_3) + Q_{bs}\cos(k_r x_2 + k_s x_3) \end{aligned} \tag{A.8}$$

and

$$\begin{aligned} S_{33} = {} & \left(\frac{\gamma - 1}{\gamma}\right)^2 (S_{aa} + S_{bb} + 2C_{ab}\cos(k_i + k_r)x_3 \\ & - 2Q_{ab}\sin(k_i + k_r)x_3) + \frac{2(\gamma - 1)}{\gamma}(C_{as}\cos(k_i - k_s)x_3 \\ & - Q_{as}\sin(k_i - k_s)x_3 + C_{bs}\cos(k_r + k_s)x_3 \\ & - Q_{bs}\sin(k_r + k_s)x_3) + S_{ss} \end{aligned} \tag{A.9}$$

Acknowledgments

The authors acknowledge the assistance of Will Moase with some of the data postprocessing and the validation of the 2M1T method.

References

[1] Rayleigh, Lord, *The Theory of Sound*, Macmillan and Co., London, Vol. 2, 1896.
[2] Culick, F. E. C., "Combustion Instabilities in Propulsion Systems," *Winter Annual Meeting of the ASME*, ASME, San Francisco, 1989.
[3] Lieuwen, T., "Modeling Premixed Combustion-Acoustic Wave

Interactions: A Review," *Journal of Propulsion and Power*, Vol. 19, No. 5, 2003, pp. 765–781.
[4] MacQuisten, M. A., and Dowling, A. P., "Low-Frequency Combustion Oscillations in a Model Afterburner," *Combustion and Flame*, Vol. 94, Aug. 1993, pp. 253–264. doi:10.1016/0010-2180(93)90072-B
[5] Dowling, A. P., "Acoustics of Unstable Flows," *XIXth International Congress of Theoretical and Applied Mechanics*, Elsevier Science, New York, 1997.
[6] Hield, P. A., Brear, M. J., and Moase, W. H., "A Parametric, Linear Stability Analysis of Thermoacoustic Oscillations," *2003 Australian Symposium on Combustion & The 8th Australian Flame Days*, Monash University, 2003.
[7] Marble, F. E., and Candel, S. M., "Acoustic Disturbance from Gas Non-Uniformities Convected Through a Nozzle," *Journal of Sound and Vibration*, Vol. 55, No. 2, 1977, pp. 225–243. doi:10.1016/0022-460X(77)90596-X
[8] Bloxsidge, G. J., Dowling, A. P., and Langhorne, P. J., "Reheat Buzz: An Acoustically Coupled Combustion Instability. Part 2. Theory," *Journal of Fluid Mechanics*, Vol. 193, Aug. 1988, pp. 445–473. doi:10.1017/S0022112088002216
[9] Keller, J. J., "Thermoacoustic Oscillations in Combustion Chambers of Gas Turbines," *AIAA Journal*, Vol. 33, No. 12, 1995, pp. 2280–2287.
[10] Eckstein, J., Freitag, E., Hirsch, C., and Sattelmayer, T., "Experimental Study on the Role of Entropy Diffusion Waves in Low-Frequency Oscillations for a Diffusion Burner," *Proceedings of the ASME Turbo Expo 2004: Power for Land, Sea, and Air*, ASME, Fairfield, NJ, 2004.
[11] Seybert, A. F., and Ross, D. F., "Experimental Determination of Acoustic Properties Using a Two-Microphone Random-Excitation Technique," *Journal of the Acoustical Society of America*, Vol. 61, No. 5, 1977, pp. 1362–1370. doi:10.1121/1.381403
[12] Hield, P. A., "A Theoretical and Experimental Investigation of Thermoacoustic Instability in a Turbulent Premixed Laboratory Combustor," Ph.D. Thesis, University of Melbourne, Victoria, Australia, 2007.
[13] Dowling, A. P., "The Calculation of Thermoacoustic Oscillations," *Journal of Sound and Vibration*, Vol. 180, No. 4, 1995, pp. 557–581. doi:10.1006/jsvi.1995.0100
[14] Heitor, M. V., Taylor, A. M. K. P., and Whitelaw, J. H., "Influence of Confinement on Combustion Instabilities of Premixed Flames Stabilized on Axisymmetric Baffles," *Combustion and Flame*, Vol. 57, July 1984, pp. 109–121. doi:10.1016/0010-2180(84)90141-X
[15] Ffowcs Williams, J. E., and Howe, M. S., "The Generation of Sound by Density Inhomogeneities in Low Mach Number Nozzle Flows," *Journal of Fluid Mechanics*, Vol. 70, No. 3, 1975, pp. 605–622. doi:10.1017/S0022112075002224
[16] Dowling, A. P., and Stow, S. R., "Acoustic Analysis of Gas Turbine Combustors," *Journal of Propulsion and Power*, Vol. 19, No. 5, 2003, pp. 751–764.
[17] Chung, J. Y., and Blaser, D. A., "Transfer Function Method of Measuring In-Duct Acoustic Properties. I. Theory," *Journal of the Acoustical Society of America*, Vol. 68, No. 3, 1980, pp. 907–921. doi:10.1121/1.384778
[18] Eldredge, J. D., and Dowling, A. P., "The Absorption of Axial Acoustic Waves by a Perforated Liner with Bias Flow," *Journal of Fluid Mechanics*, Vol. 485, June 2003, pp. 307–335. doi:10.1017/S0022112003004518
[19] Jeong, K.-W., and Ih, J.-H., "A Numerical Study on the Propagation of Sound Through Capillary Tubes with Mean Flow," *Journal of Sound and Vibration*, Vol. 198, No. 1, 1996, pp. 67–79. doi:10.1006/jsvi.1996.0557
[20] Newland, D. E., *Random Vibrations, Spectral and Wavelet Analysis*, Longman Scientific and Technical, Marlow, 1993.
[21] Bendat, J. S., and Piersol, A. G., *Engineering Applications of Correlation and Spectral Analysis*, Wiley, New York, 1980.
[22] The Mathworks, MATLAB Signal Processing Toolbox 6 User's Guide, The Mathworks, Natick, MA, 2007.
[23] Dawson, S., and Fitzpatrick, J. A., "Measurement and Analysis of Thermoacoustic Oscillations in a Simple Dump Combustor," *Journal of Sound and Vibration*, Vol. 230, No. 3, 2000, pp. 649–660. doi:10.1006/jsvi.1999.2633
[24] Langhorne, P. J., "Reheat Buzz: An Acoustically Coupled Combustion Instability. Part 1. Experiment," *Journal of Fluid Mechanics*, Vol. 193, Aug. 1988, pp. 417–443. doi:10.1017/S0022112088002204
[25] Poinsot, T. J., Trouve, A. C., Veynante, D. P., Candel, S. M., and Esposito, E. J., "Vortex-Driven Acoustically Coupled Combustion Instabilities," *Journal of Fluid Mechanics*, Vol. 177, April 1987, pp. 265–292. doi:10.1017/S0022112087000958
[26] Seybert, A. F., and Soenarko, B., "Error Analysis of Spectral Estimates with Application to the Measurement of Acoustic Parameters Using Random Sound Fields in Ducts," *Journal of the Acoustical Society of America*, Vol. 69, No. 4, 1981, pp. 1190–1199. doi:10.1121/1.385700
[27] Boden, H., and Abom, M., "Influence of Errors on the Two-Microphone Method for Measuring Acoustic Properties in Ducts," *Journal of the Acoustical Society of America*, Vol. 79, No. 2, 1986, pp. 541–549. doi:10.1121/1.393542
[28] Moase, W. H., Brear, M. J., and Manzie, C., "The Forced Response of Choked Nozzles and Supersonic Diffusers," *Journal of Fluid Mechanics* (to be published).

T. Jackson
Associate Editor